IEEE Access
Multidisciplinary | Rapid Review | Open Access Journal

Received May 12, 2020, accepted May 20, 2020, date of publication May 29, 2020, date of current version June 10, 2020.

Digital Object Identifier 10.1109/ACCESS.2020.2998488

Practical Design and Implementation Method for Asymmetric-Response Post-Loaded Substrate-Integrated Waveguide Filters

SANGGU LEE, SEUNGGOO NAM, AND JUSEOP LEE, (Senior Member, IEEE)
Department of Computer and Radio Communications Engineering, Korea University, Seoul 02841, South Korea

Corresponding author: Juseop Lee (juseoplee@gmail.com)

This work was supported by the National Research Foundation of Korea (NRF) under Grant NRF-2018R1A2B6006095.

ABSTRACT This paper presents a practical method for implementing a post-loaded substrate-integrated waveguide (SIW) filter producing an asymmetric response with a pair of near-band transmission zeros. More specifically, we present a practical frequency-dependent coupling structure for post-loaded SIW resonators for implementing an asymmetric response. By virtue of the proposed coupling design methods, the roll-offs in the upper and lower stopbands can be readily controlled to be different from each other. In other words, the roll-off in a stopband can be made to be steeper than the one in the other stopband by means of using the proposed design method for coupling structure. More importantly, we propose a useful approach to swap the two stopband responses of an asymmetric-response filter. In other word, this paper shows a practical method to laterally reverse an asymmetric response. For demonstration, 1 symmetric-response and 2 asymmetric-response fourth-order SIW filters have been designed using the presented frequency-dependent coupling structures.

INDEX TERMS Coupling, filter, resonator, substrate-integrated waveguide.

I. INTRODUCTION

In general, transmission zeros are employed in bandpass filter designs to have steep roll-off responses in the stopbands. There are many available techniques for producing transmission zeros, and one of them is using a single or multiple cross couplings. For example, it is well known that a third-order filter with a cross coupling between the first and third resonators can have a transmission zero in either lower or upper stopband depending on the sign of the cross coupling. In addition, a fourth-order filter can be designed to have a pair of transmission zeros by having a cross coupling between the first and fourth resonators. The synthesis of a filter with cross couplings can be carried out by using the concept of the coupling matrix. Overall, the concept of the coupling matrix with constant coupling values has been extensively utilized in designing cross-coupled resonator filters, as the assumption that the coupling values are constant makes the filter synthesis practical.

Separately, filter synthesis and design methods incorporating frequency-dependent couplings have been of great interest as they allow us to have more capabilities [1]–[17]. For example, additional transmission zeros can be implemented by using a frequency-dependent coupling. In [1]–[5], the synthesis of filters with one or multiple frequency-dependent couplings are reported. It is shown in [6]–[8] that microstrip-line filters having frequency-dependent couplings can generate additional transmission zeros. In addition, frequency-dependent couplings in various filter structures such as standard and substrate-integrated waveguide filters can be found in [9]–[17].

Although a great amount of research has been done on frequency-dependent couplings, their applications to the design of asymmetric-response post-loaded SIW filters have rarely been reported. In addition, producing various types of asymmetric filtering responses using a post-loaded SIW filter structure has not been reported. More importantly, a method for obtaining a laterally-reversed image response of an asymmetric response of a post-loaded SIW filter has not been available up to date. This work, for the first time, shows that there is no need to change the sign of the slope of the coupling value in laterally reversing a frequency response to produce its image response. For demonstration,

The associate editor coordinating the review of this manuscript and approving it for publication was Feng Lin.

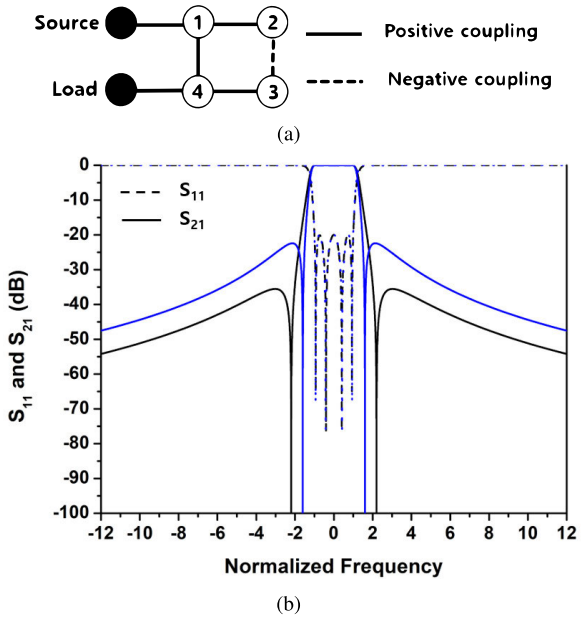

FIGURE 1. (a) Coupling diagram of a fourth-order filter with a cross coupling between resonators 1 and 4. (b) Frequency response corresponding to (4) (black line) and the one when the transmission zeros are closer to the passband (blue line).

we will first show the design of a fourth-order cross-coupled symmetric-response post-loaded SIW filter followed by showing the design of asymmetric-response filters. It also presents filter design examples validating that the image of an asymmetric response can be obtained without changing the slope of the frequency-dependent coupling value.

II. COUPLING MATRIX SYNTHESIS

Fig. 1(a) shows the coupling diagram of a fourth-order filter with a cross-coupling between resonators 1 and 4, and the corresponding matrix is given by

$$\mathbf{M} = \begin{bmatrix} 0 & M_{01} & 0 & 0 & 0 & 0 \\ M_{01} & M_{11} & M_{12} & 0 & M_{14} & 0 \\ 0 & M_{12} & M_{22} & M_{23} & 0 & 0 \\ 0 & 0 & M_{23} & M_{33} & M_{34} & 0 \\ 0 & M_{14} & 0 & M_{34} & M_{44} & M_{45} \\ 0 & 0 & 0 & 0 & M_{45} & 0 \end{bmatrix} \tag{1}$$

In this paper, the number of rows and columns of all matrices starts from 0 to be consistent with (1). The coupling values in the coupling matrix can be found by well-known synthesis methods [18]–[20]. As the filter synthesis process is widely known, this paper only discusses its summary. The immittance matrix of a inverter-coupled filter network is

$$\mathbf{A} = \mathbf{P} + jw\mathbf{U} + j\mathbf{M} \tag{2}$$

where w is the normalized frequency, $\mathbf{P}$ is a matrix whose only nonzero entries are $\mathbf{P}_{(0,0)} = \mathbf{P}_{(5,5)} = 1$, and $\mathbf{U}$ is the identity matrix except for $\mathbf{U}_{(0,0)} = \mathbf{U}_{(5,5)} = 0$. The corresponding S-parameters are

$$\begin{aligned} |S_{11}(w)| &= |2\mathbf{A}^{-1}{}_{(0,0)} - 1| \\ |S_{21}(w)| &= |2\mathbf{A}^{-1}{}_{(5,0)}| \end{aligned} \tag{3}$$

Using (1)-(3) and the predefined transfer function, the coupling matrix can be found. For example, the coupling matrix for producing the pseudo-elliptic response with 20 dB equi-ripple return loss and a pair of transmission zeros at ± 2.2 in the normalized frequency domain depicted by the black lines in Fig. 1(b) is given by

$$\mathbf{M} = \begin{bmatrix} 0 & 1.026 & 0 & 0 & 0 & 0 \\ 1.026 & 0 & 0.880 & 0 & 0.137 & 0 \\ 0 & 0.880 & 0 & -0.754 & 0 & 0 \\ 0 & 0 & -0.754 & 0 & 0.880 & 0 \\ 0 & 0.137 & 0 & 0.880 & 0 & 1.026 \\ 0 & 0 & 0 & 0 & 1.026 & 0 \end{bmatrix} \tag{4}$$

The coupling matrix in (4) has a negative coupling between resonators 2 and 3, but any inter-resonator coupling out of 4 can be a negative one for producing the same response [21]. By virtue of the transmission zeros, the response has sharp roll-offs. When the transmission zeros are closer to the passband, the roll-offs become sharper while the rejection levels at frequencies outside of the transmission zeros decrease as depicted by the blue lines in Fig. 1(b). In other words, the roll-offs become steeper and the humps next to the transmission zeros rise as the zeros are placed closer to the passband. As the frequency response shown in Fig. 1(b) is symmetric, responses in the upper and lower stopbands are the same. In a case where a filter is required to have different roll-offs and rejection levels limited by the humps in the upper and lower stopbands, a filter must be designed to have an asymmetric response.

In this work, we propose to make the cross-coupling value dependent on the frequency on purpose, as it turns a symmetric response into an asymmetric one to a greater extent in comparison with frequency-dependent direct couplings. We can make the roll-offs and hump levels in the two stopbands different from each other by replacing a frequency-independent cross-coupling with a frequency-dependent one. Under the assumption that a frequency-dependent cross-coupling value varies linearly with the normalized frequency, $\mathbf{U}$ in (2) can be generalized to

$$\mathbf{U} = \begin{bmatrix} 0 & 0 & 0 & 0 & 0 & 0 \\ 0 & 1 & 0 & 0 & U_{14} & 0 \\ 0 & 0 & 1 & 0 & 0 & 0 \\ 0 & 0 & 0 & 1 & 0 & 0 \\ 0 & U_{14} & 0 & 0 & 1 & 0 \\ 0 & 0 & 0 & 0 & 0 & 0 \end{bmatrix} \tag{5}$$

where U_{14} is the rate of change (slope) of the cross-coupling value. Hence, the synthesis of an asymmetric-response filter containing a frequency-dependent cross-coupling involves finding the coupling matrix in (1) and the slope U_{14}. Again, as the works on the synthesis of a filter with frequency-dependent couplings can also be found extensively in the literature [1]–[17], this paper will briefly describe the filter synthesis. If a filter has a frequency-dependent cross-coupling, it can have one more transmission zero. Hence,

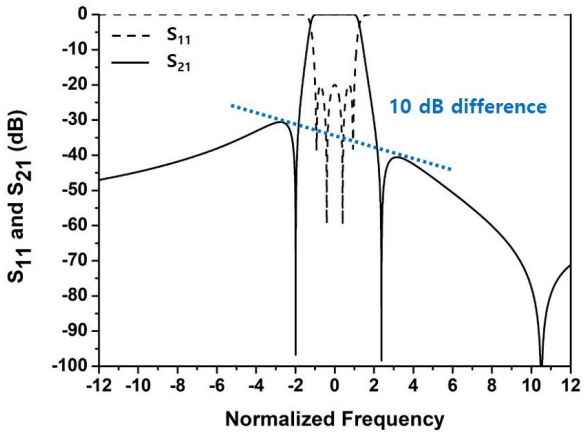

FIGURE 2. Asymmetric frequency response corresponding to (6).

three transmission zeros must be in use in the process of predefining a desired filter response. For example, the frequency response shown in Fig. 2 has three transmission zeros at $w_{z1} = -1.985$, $w_{z2} = +2.38$, $w_{z3} = +10.5$. The roll-offs in the lower and upper stopbands are different from each other and the response has different minimum rejections limited by the humps next to the two transmission zeros at w_{z1} and w_{z2}. Compared to the response in Fig. 1(b), the response in Fig. 2 has a steeper roll-off in the lower stopband and a shallower roll-off in the upper stopband. Due to the asymmetric transmission zeros, it has 5 dB less rejection in the lower stopband and 5 dB more rejection in the upper stopband, which leads to 10 dB difference in near-band rejections. We can find the coupling matrix and the slope of the cross-coupling value producing the frequency response in Fig. 2 and they are given by

$$\mathbf{M} = \begin{bmatrix} 0 & 1.025 & 0 & 0 & 0 & 0 \\ 1.025 & 0.006 & 0.877 & 0 & 0.147 & 0 \\ 0 & 0.877 & 0.009 & -0.758 & 0 & 0 \\ 0 & 0 & -0.758 & -0.001 & 0.877 & 0 \\ 0 & 0.147 & 0 & 0.877 & -0.01 & 1.025 \\ 0 & 0 & 0 & 0 & 1.025 & 0 \end{bmatrix}$$
$$U_{14} = -0.0135 \tag{6}$$

Similarly, we can also have a larger difference in roll-offs and hump levels. The response shown in Fig. 3 has three transmission zeros at $w_{z1} = -1.783$, $w_{z2} = +2.45$, $w_{z3} = +5.513$. It has 10 dB less rejection in the lower stopband and 10 dB more rejection in the upper stopband when compared to the one in Fig. 1(b), and the coupling matrix and the slope of the cross-coupling value can be found as

$$\mathbf{M} = \begin{bmatrix} 0 & 1.023 & 0 & 0 & 0 & 0 \\ 1.023 & -0.018 & 0.869 & 0 & 0.176 & 0 \\ 0 & 0.869 & 0.005 & -0.769 & 0 & 0 \\ 0 & 0 & -0.769 & 0.01 & 0.869 & 0 \\ 0 & 0.176 & 0 & 0.869 & -0.006 & 1.023 \\ 0 & 0 & 0 & 0 & 1.023 & 0 \end{bmatrix}$$
$$U_{14} = -0.0284 \tag{7}$$

So far, we have shown the frequency responses whose roll-off in the lower stopband is steeper than the one in the upper stopband. In these cases, the minimum rejection level limited by the hump in the lower stopband is smaller than the one in the upper stopband due to the asymmetrically positioned transmission zeros. Seperately, we can also synthesize the responses with the opposite behavior. For example, Fig. 4 and Fig. 5 show the images of the responses

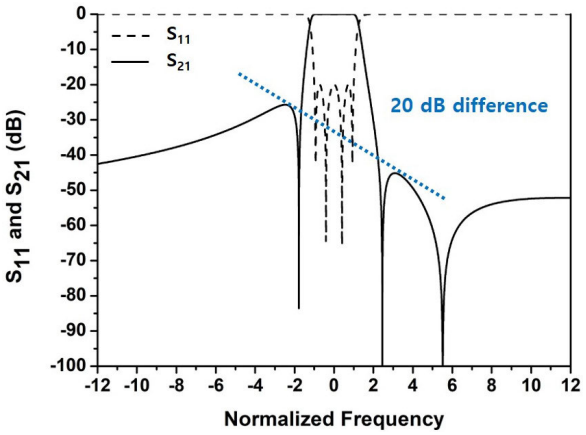

FIGURE 3. Asymmetric frequency response corresponding to (7).

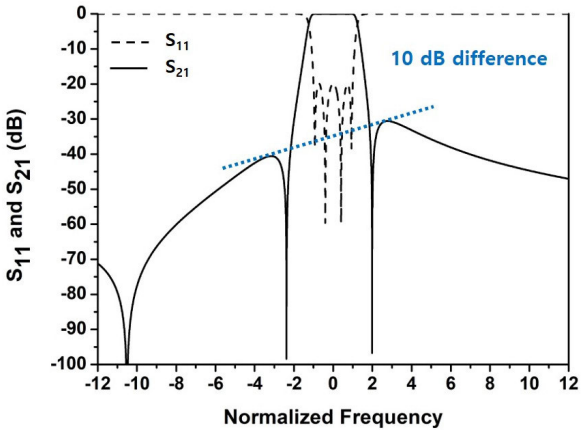

FIGURE 4. Asymmetric frequency response corresponding to (12).

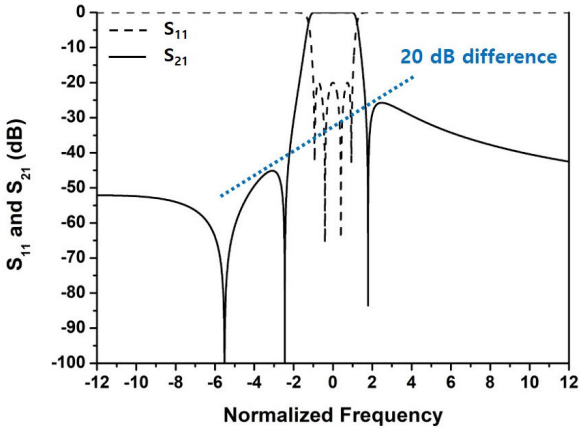

FIGURE 5. Asymmetric frequency response corresponding to (13).

in Fig. 2 and Fig. 3, respectively. The filters having the image responses shown in Fig. 4 and Fig. 5 can be directly synthesized using the relationship between the immittance matrix **A** and the S-parameters in (3). On the other hand, the image responses can be obtained by changing the sign of all elements of the coupling matrices in (6) and (7) which leads to [22]

$$\mathbf{M} = \begin{bmatrix} 0 & -1.025 & 0 & 0 & 0 & 0 \\ -1.025 & -0.006 & -0.877 & 0 & -0.147 & 0 \\ 0 & -0.877 & -0.009 & 0.758 & 0 & 0 \\ 0 & 0 & 0.758 & 0.001 & -0.877 & 0 \\ 0 & -0.147 & 0 & -0.877 & 0.01 & -1.025 \\ 0 & 0 & 0 & 0 & -1.025 & 0 \end{bmatrix}$$
$$U_{14} = -0.0135 \tag{8}$$

$$\mathbf{M} = \begin{bmatrix} 0 & -1.023 & 0 & 0 & 0 & 0 \\ -1.023 & 0.018 & -0.869 & 0 & -0.176 & 0 \\ 0 & -0.869 & -0.005 & 0.769 & 0 & 0 \\ 0 & 0 & 0.769 & -0.01 & -0.869 & 0 \\ 0 & -0.176 & 0 & -0.869 & 0.006 & -1.023 \\ 0 & 0 & 0 & 0 & -1.023 & 0 \end{bmatrix}$$
$$U_{14} = -0.0284 \tag{9}$$

For reducing the number of negative couplings, the concept of the matrix transformation [21] can be applied to (8) and (9). The matrix transformation for changing the sign of elements is given by

$$\mathbf{M}' = \mathbf{R} \cdot \mathbf{M} \cdot \mathbf{R}^{-1} \tag{10}$$

where **R** is identical to the identity matrix except that some of its diagonal elements are -1. The sign of the off-diagonal elements in the *i*th row and column can be changed when *i*th diagonal element of **R** is -1. Hence, by applying the matrix transformation with

$$\mathbf{R}_{(1,1)} = \mathbf{R}_{(4,4)} = -1 \tag{11}$$

to (8) and (9) gives

$$\mathbf{M} = \begin{bmatrix} 0 & 1.025 & 0 & 0 & 0 & 0 \\ 1.025 & -0.006 & 0.877 & 0 & -0.147 & 0 \\ 0 & 0.877 & -0.009 & 0.758 & 0 & 0 \\ 0 & 0 & 0.758 & 0.001 & 0.877 & 0 \\ 0 & -0.147 & 0 & 0.877 & 0.01 & 1.025 \\ 0 & 0 & 0 & 0 & 1.025 & 0 \end{bmatrix}$$
$$U_{14} = -0.0135 \tag{12}$$

$$\mathbf{M} = \begin{bmatrix} 0 & 1.023 & 0 & 0 & 0 & 0 \\ 1.023 & 0.018 & 0.869 & 0 & -0.176 & 0 \\ 0 & 0.869 & -0.005 & 0.769 & 0 & 0 \\ 0 & 0 & 0.769 & -0.01 & 0.869 & 0 \\ 0 & -0.176 & 0 & 0.869 & 0.006 & 1.023 \\ 0 & 0 & 0 & 0 & 1.023 & 0 \end{bmatrix}$$
$$U_{14} = -0.0284 \tag{13}$$

The matrix transformation using matrix R in (10) has also been applied to matrix **U** in (5) when transforming the matrices in (8) and (9) to the ones in (12) and (13), respectively. However, it is worth noting that this process does not change the sign of U_{14} as shown in (12) and (13). This indicates that the image response of an asymmetric response can be obtained without changing the slope of the frequency-dependent cross-coupling value.

III. PRACTICAL DESIGN

In this section, we present a practical method for implementing a frequency-dependent coupling structure suited for post-loaded SIW resonators. For demonstrating the practicality of the coupling structure presented in this section, it has been applied to the design of asymmetric-response filters centered at 4.5 GHz with the bandwidth of 285 MHz. Two filters have been designed using the matrices in (7) and (13) targeting to produce the frequency responses in Fig. 3 and Fig. 5, as they have a higher degree of asymmetry in comparison with the ones in Fig. 2 and Fig. 4.

A. RESONATOR

Fig. 6 shows the substrate-integrated waveguide resonator structure used in our filter design. As filter designs using this type of resonator structure have been extensively reported [23]–[27], this paper briefly describes the resonator structure rather than discussing its detailed operating principle and design method. The resonator is contained in two substrates and its side walls are formed by creating via holes running from the top conductive surface to the bottom conductive surface. There exists a conducting post made with a circular patch and ten vias in the TMM3 substrate. The diameter of the vias are all determined to be 0.5 mm. The air gap exists above the post due to the empty space of a FR4 substrate and the electric field of the resonator is mainly confined in this air gap. As the structure composed of the circular patch of the post, the top conductive surface, and the air gap between them behaves like an air-filled capacitor, it is possible to fine-tune

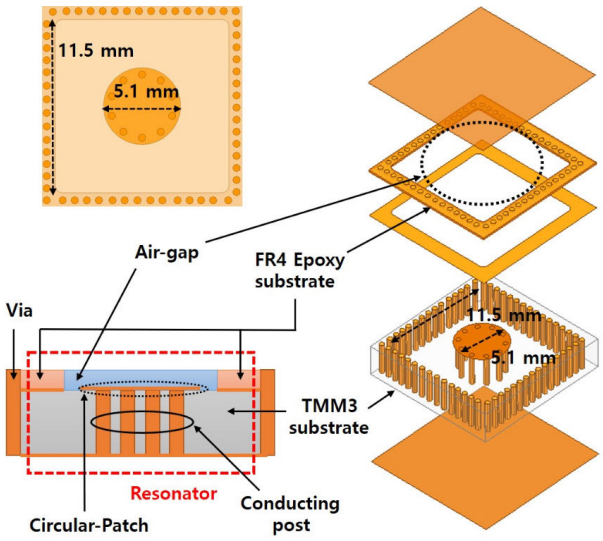

FIGURE 6. Cross-sectional view and the layer-by-layer view of the resonator.

the center frequency after fabrication by changing the air-gap thickness. The side length of the resonator and the diameter of the circular patch are determined to have 11.5 mm and 5.1 mm, respectively, so that the resonator can resonate at 4.5 GHz.

B. COUPLING STRUCTURES

In our filter designs, we use one type of external coupling structure and two different types of interresonator coupling structures. Fig. 7(a) shows the external coupling structure between the post-loaded SIW resonator and the GCPW (grounded coplanar waveguide) port, and Fig. 7(b) shows the iris between the two resonators. The external coupling value increases when the rounded slots surrounding the post are elongated and the coupling value of the iris increases with its width. The sign of interresonator coupling itself is of no importance and it is relative. Hence, in this paper, we define the sign convention by assigning the positive sign to the iris. As the coupling structures in Fig. 7 can be designed in such a way as to have target coupling values by following traditional standard methods reported in the literature including [28]–[31], the detailed discussions on them are not repeated in this paper. On the other hand, this paper focuses on the interresonator coupling structure shown in Fig. 8. The coupling structure shown in Fig. 8 has an S-shaped conductive strip and an iris. This type of structure was reported to be a frequency-independent negative coupling [32], but this paper, for the first time, demonstrates that it can be used as not only a frequency-independent coupling structure but also a frequency-dependent coupling allowing for designing an asymmetric-response post-loaded SIW filter. It will be shown that the coupling structure in Fig. 8 is flexible enough to implement the frequency-dependent coupling values in (7) and (13). More specifically, this work will show that the slope

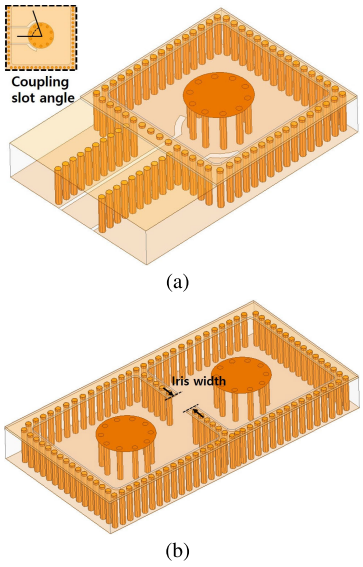

FIGURE 7. (a) Resonator with external coupling. (b) Iris between two resonators.

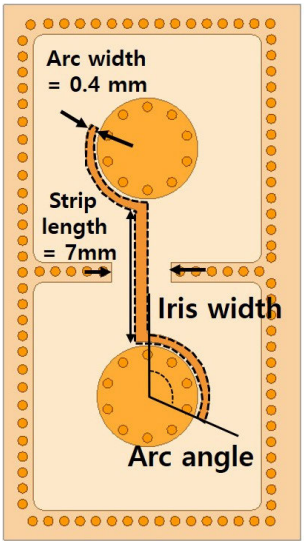

FIGURE 8. Interresonator coupling with an S-shaped conductive strip.

of the coupling value of the coupling structure can be adjusted so as to implement the target values.

A conventional method to find the coupling value of a coupling structure is based on simulating the coupled resonators that are excited by weak external couplings [22]. The simulated transmission response has two resonant peaks and the normalized coupling value can be derived from their resonant frequencies, f_1 and f_2, as follows:

$$M = \pm \frac{|f_2 - f_1|}{BW} \tag{14}$$

However, this method is not perfectly suited for finding the frequency-dependent coupling value. This is because the transmission zero generated by the frequency-dependent coupling structure is used in calculating the slope of the coupling value but it is rarely observed when using the conventional method. Hence, we simulated the coupled resonators that are individually coupled to the port with a very low impedance as suggested in [33]. Fig. 9 shows two examples of the transmission response of the coupled-resonator structure shown in Fig. 8 with the resonators coupled to low-impedance ports. Two resonant peaks at f_1 and f_2 and a transmission zero at f_z can be observed, and we can extract the coupling value and its slope. The coupling value can be obtained by (14) and its slope is given by [3]

$$U = -\Delta \cdot \frac{M}{(f_z/f_0) - (f_0/f_z)} \tag{15}$$

where Δ denotes the fractional bandwidth.

There are many physical dimensions that can be used as design parameters for achieving the desired coupling value at the center frequency and its slope. In this design, we control the iris width and the arc angle of the strip while the others are set to constants as shown in Fig. 8. For example, the coupling value and its slope in (7) are 0.176 and -0.0284. The target coupling value can be realized by numerous pairs of the iris

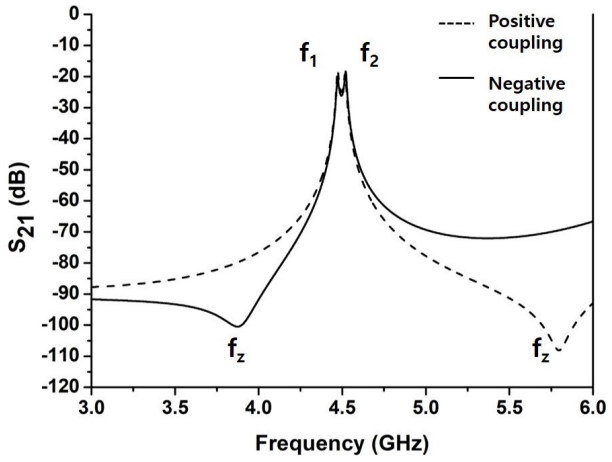

FIGURE 9. Simulated S_{21} response for the positive coupling (dashed line) and the negative coupling (solid line).

width and the arc angle of the strip. In general, if a pair of the two parameters gives the target coupling value, then another pair can be found by increasing both two parameters. The horizontal axis of Fig. 10 shows the pairs of the two design parameters producing the target coupling value in (7). However, each pair gives a different slope of the coupling value and Fig. 10 shows the variation of the slope of the coupling value with the two design parameters. Hence, the two design parameters can be determined by finding the target slope of the coupling value on the y-axis followed by reading the corresponding design parameters on the x-axis. According to Fig. 10, the iris width and the arc angle have been chosen to be 5 mm and 83 degrees, respectively for having the target coupling value and its slope. Similarly, the two design parameters can also be found to have a different set of target coupling value and its slope for producing a different response. For example, we can also produce the image response in Fig. 5 by means of designing the frequency-dependent coupling structure in such a way as to have the target coupling value and its slope in (13). The horizontal axis of Fig. 11 shows the pairs of the two design parameters producing the targeted coupling

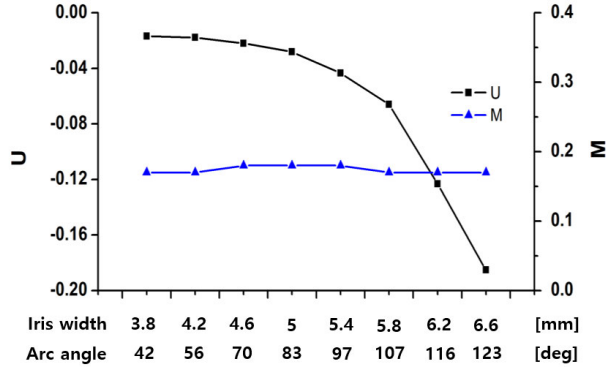

FIGURE 10. Design graphs for (7). (Variations of U_{14} and M_{14} with respect to the iris width and the arc angle).

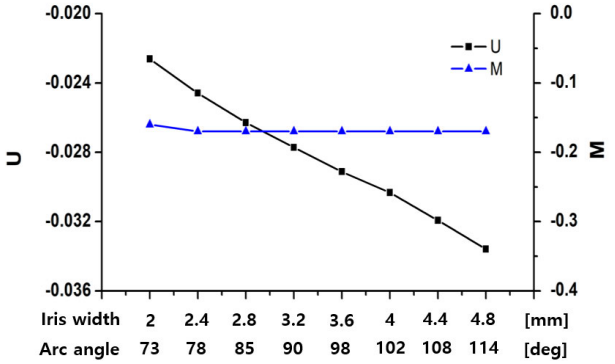

FIGURE 11. Design graph for (13). (Variations of U_{14} and M_{14} with respect to the iris width and the arc angle).

value in (13) given by -0.176. The slope of the coupling value can be extracted using (15) and it is shown in Fig. 11. It can be concluded that the iris width and the arc angle of the strip are required to be 3.2 mm and 90 degrees, respectively, to have the target slope of the coupling value, -0.0284.

C. FILTER DESIGN

Fig. 12 shows the top views of the TMM substrate of the filters designed using the coupling matrices in (4), (7), and (13). The design of the filters is based on the assumption that the direct couplings are frequency-independent couplings. This is because, as mentioned earlier, the coupling value variation of the direct couplings has a negligible impact on the frequency response in comparison with the cross coupling. For the purpose of the convenient comparison, all filters are designed to have the same center frequency and bandwidth that are 4.5 GHz and 285 MHz, respectively. Fig. 12(a) is

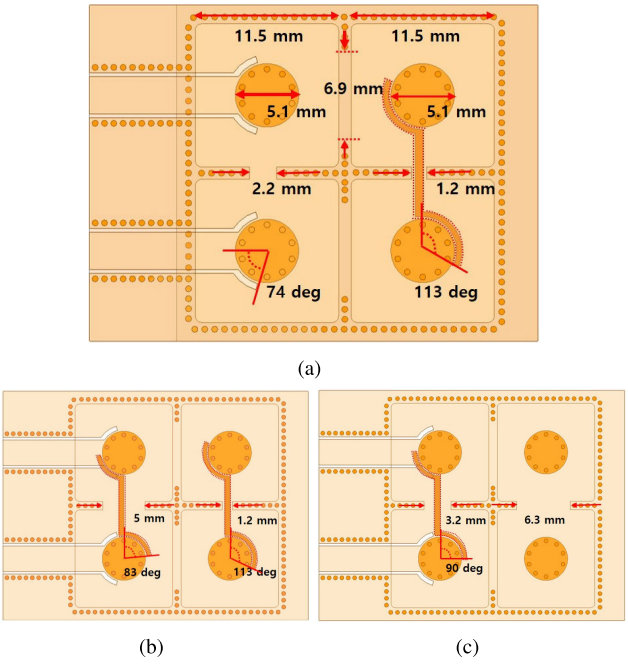

FIGURE 12. Physical dimensions. (a) filter corresponding to (4). (b) filter corresponding to (7). (c) filter corresponding to (13).

the filter corresponding to the coupling matrix in (4) producing the symmetric response shown in Fig. 1(b). Three irises are employed to implement three positive interresonator couplings. On the other hand, a negative coupling presented in [32] is formed between resonators 2 and 3 by means of using the S-shaped conductive strip. As mentioned previously, multiple sets of the two design parameters, the iris width and the angle of the arc of the strip, can be found for having the target coupling value. In this design, the two design parameters have been chosen to be as small as possible in order to have a small coupling value variation with respect to the frequency, although the frequency dependence of the direct coupling value does not have a great impact on the frequency response. If necessary, a negative coupling value different from the one in (4) can also be implemented by simply changing the arc angle of the conductive strip. Fig. 13 shows the layer-by-layer view of the filter shown in Fig. 12(a). The solid lines in Fig. 14 and Fig. 15 show the simulated transmission and reflection responses of the filter.

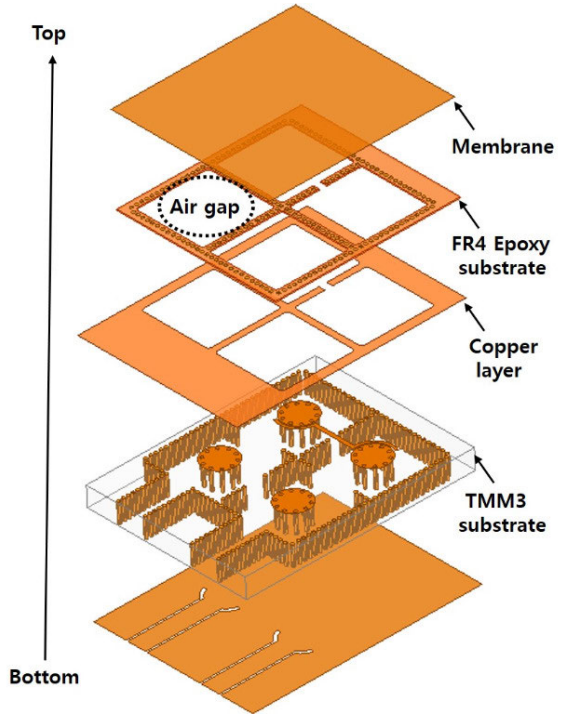

FIGURE 13. Layer-by-layer view of proposed structure.

Figs. 12(b) shows the top view of the TMM3 substrate of the filter designed by using the coupling matrix in (7) for producing the asymmetric response in Fig. 3. The dimensions of the coupling structures have been determined by the design method discussed in the previous section in a way to have the target coupling. It is worth noting that the frequency-dependent coupling structure shown in Fig. 8 is placed between resonators 1 and 4 in order to realize the frequency-dependent cross-coupling value given in (7). The dotted lines in Fig. 14 depict the simulated response of filter. The filter has an asymmetric response with a steeper roll-off in the lower stopband and a shallower roll-off in the upper stopband, as intended. It is shown that two hump levels of the filter are different from each other as intended due to the asymmetric transmission zeros.

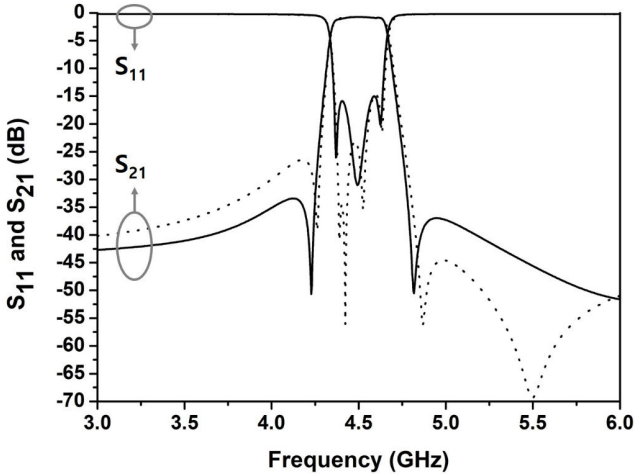

FIGURE 14. Solid lines and dotted lines show simulated responses of filters corresponding to (4) and (7), respectively.

The top view of the filter designed by using the coupling matrix in (13) is shown in Fig. 12(c). The filter is intended to have the frequency response in Fig. 5. The filter has the presented frequency-dependent coupling structure between resonators 1 and 4. The simulated response of the filter is depicted by the dotted lines in Fig. 15. It is shown that the filter has an asymmetric response due to the fact that the transmission zero in the upper stopband is closer to the passband while the one in the lower stopband is farther when compared with zeros in the symmetric response.

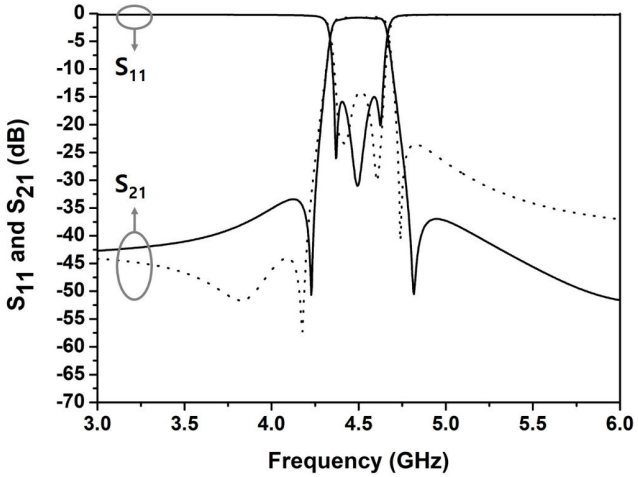

FIGURE 15. Solid lines and dotted lines show simulated responses of filters corresponding to (4) and (13), respectively.

IV. MEASUREMENT AND DISCUSSION

For verifying the proposed frequency-dependent coupling structure and the design method for an asymmetric-response

TABLE 1. Comparison between this work with previous works.

	Frequency-dependent coupling value in cross coupling	Response type	Slope control maintaining coupling value	Laterally-reversed image response
[1]	Yes	Asymmetric	No	No
[2]	Yes	Asymmetric	No	No
[3]	Yes	Asymmetric	No	No
[4]	No	Asymmetric	No	No
[5]	No	Symmetric, Asymmetric	No	No
[6]	Yes	Symmetric, Asymmetric	No	No
[7]	Yes	Symmetric	No	No
[8]	Yes	Asymmetric	No	No
[9]	No	Asymmetric	No	No
[10]	Yes	Asymmetric	No	No
[11]	Yes	Asymmetric	No	No
[12]	Yes	Asymmetric	No	No
[13]	Yes	Asymmetric	No	No
[14]	Yes	Asymmetric	No	No
[15]	Yes	Symmetric	No	No
[16]	Yes	Asymmetric	No	No
[17]	No	Symmetric	No	No
This work	**Yes**	**Asymmetric**	**Yes**	**Yes**

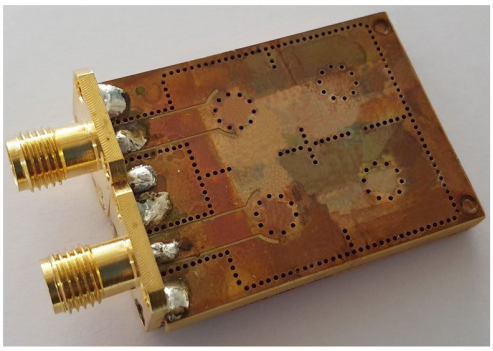

FIGURE 16. Photograph of the fabricated filter.

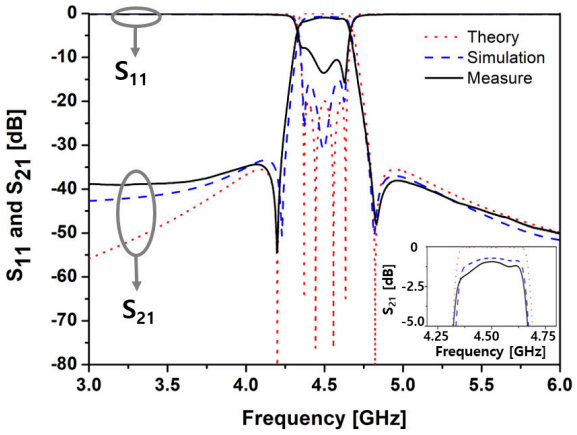

FIGURE 17. Frequency responses of filter corresponding to (4).

post-loaded SIW resonator filter, the three filters discussed in the previous section have been fabricated and measured. All filters are made with two substrates (Rogers TMM3 and FR4) and Fig. 16 shows one of the fabricated filters. The structures have been fabricated by using commercially available etching, drilling and plating processes. Fig. 17 shows

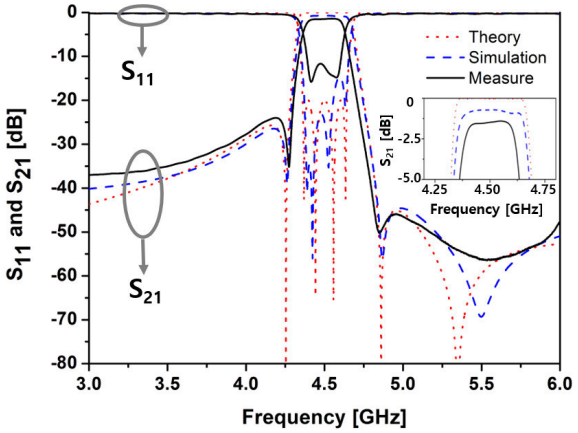

FIGURE 18. Frequency responses of filter corresponding to (7).

the frequency responses of the symmetric-response filter. The theoretical, simulated, and measured responses agree well with one another. As the two transmission zeros are placed symmetrically with respect the center frequency, the roll-offs in the lower and upper stopbands are almost identical. In addition, the levels of the two humps next to the transmission zeros are almost the same by virtue of the symmetric transmission zeros. Figs. 18 shows the theoretical, simulated, and measured frequency responses of the asymmetric-response filter designed using the coupling matrix and the slope of the cross-coupling value in (7). The filter has a steeper roll-off in the low stopband, as intended, by virtue of the transmission zeros placed asymmetrically which, in turn, are attributed to the frequency-dependent coupling between resonators 1 and 4. Fig. 19 shows the comparison between theory, simulation, and measurement of the asymmetric-response filter designed by using the coupling matrix and the slope of the cross-coupling value in (13). It is shown that the image of the response shown in Fig. 18 can be readily obtained by virtue of the presented

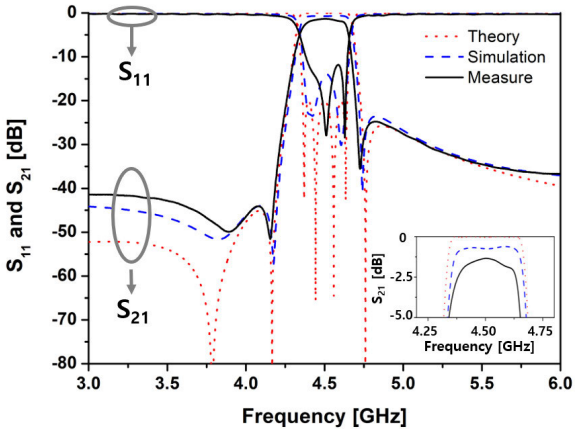

FIGURE 19. Frequency responses of filter corresponding to (13).

frequency-dependent coupling structure for post-loaded SIW resonators.

Each filter has discrepancy between simulated and measured return losses and it is mainly due to fabrication tolerance. Although the coupling structures are static ones and they were not tuned after fabrication, each filter has the in-band return loss larger than 10-12 dB overall. The measured insertion loss of the three filters at the center frequency ranges from 0.9 to 1.5 dB including the connector loss. It is believed that the measurement responses are good enough to validate the proposed practical design method for filters implementing the target asymmetric responses.

Table 1 shows the comparison between this work and the previous works on filters using the concept of frequency-dependent couplings. We believe this is the first work that presents a practical approach to implement a laterally-reversed image response using a frequency-dependent cross coupling.

V. CONCLUSION

In this paper, we have introduced a practical design approach for having an asymmetric response from a post-loaded substrate-integrated waveguide filter with a cross coupling. This work proposed to use a frequency-dependent cross coupling to produce an asymmetric frequency response. To this end, we also presented a practical frequency-dependent coupling structure suited for post-loaded SIW resonators. The fabricated filter examples successfully demonstrated the practicality of the presented coupling structure. The presented design approach using a frequency-dependent cross coupling can be expanded to using multiple cross couplings for implementing more transmission zeros. However, a suitable compromise between the number of transmission zeros and practicality must be made.

APPENDIX

This section provides examples of frequency responses demonstrating that different responses can be obtained by having the transmission zeros at different locations. The black lines in Fig. 20 show the frequency response in Fig. 3, and a different response can be obtained by moving one or multiple transmission zeros. For example, the frequency response depicted by the blue lines in Fig. 20 can be obtained by moving the transmission zero at $w_{z3} = +5.513$ to 3.5. It can be concluded that we can change the location of the transmission zero independently for the purpose of manipulating the stopband response.

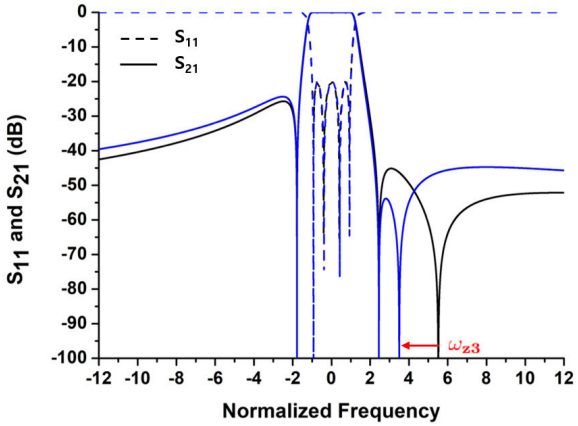

FIGURE 20. Frequency response of filter corresponding to (7) (black line) and the one of filter when the transmission zero at w_{z3} is closer to the passband (blue line).

In Section II, we demonstrated that the 20 dB difference in the rejection levels can be obtained by having 10 dB less rejection in the lower stopband and 10 dB more rejection in the upper stopband. In general, the rejection levels in the lower and upper stopbands can be adjusted independently. For example, we can have 20 dB rejection difference by reducing the lower-stopband rejection by 5 dB and increasing the upper-stopband rejection by 15 dB as shown in Fig. 21. This response can be obtained by having the three transmission zeros at $w_{z1} = -2.004$, $w_{z2} = +2.824$, and $w_{z3} = +6.315$, and the corresponding coupling matrix and the slope of the

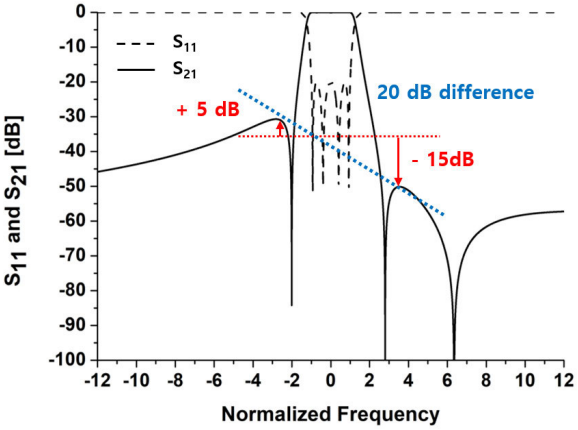

FIGURE 21. Frequency response of filter corresponding to (16).

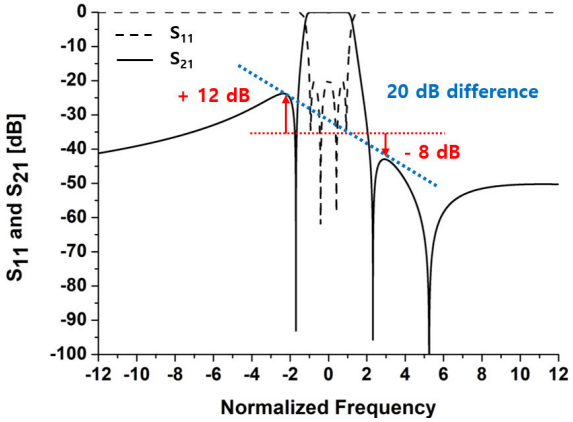

FIGURE 22. Frequency response of filter corresponding to (17).

cross-coupling value can be found as

$$\mathbf{M} = \begin{bmatrix} 0 & 1.026 & 0 & 0 & 0 & 0 \\ 1.026 & -0.014 & 0.88 & 0 & 0.132 & 0 \\ 0 & 0.88 & 0.006 & -0.752 & 0 & 0 \\ 0 & 0 & -0.752 & 0.006 & 0.88 & 0 \\ 0 & 0.132 & 0 & 0.88 & -0.004 & 1.026 \\ 0 & 0 & 0 & 0 & 1.026 & 0 \end{bmatrix}$$
$$U_{14} = -0.0184 \tag{16}$$

Furthermore, we can reduce the lower-stopband rejection by 12 dB and increase the upper-stopband rejection by 8 dB for having 20 dB difference between the two stopbands as shown in Fig. 22. The transmission zeros are at $w_{z1} = -1.692$, $w_{z2} = 2.350$, and $w_{z3} = +5.213$, and the coupling matrix and the slope of the cross-coupling values are

$$\mathbf{M} = \begin{bmatrix} 0 & 1.022 & 0 & 0 & 0 & 0 \\ 1.022 & -0.03 & 0.863 & 0 & 0.198 & 0 \\ 0 & 0.863 & 0.001 & -0.777 & 0 & 0 \\ 0 & 0 & -0.777 & 0.018 & 0.863 & 0 \\ 0 & 0.198 & 0 & 0.863 & -0.003 & 1.022 \\ 0 & 0 & 0 & 0 & 1.022 & 0 \end{bmatrix}$$
$$U_{14} = -0.0337 \tag{17}$$

REFERENCES

[1] L. Szydlowski, N. Leszczynska, and M. Mrozowski, "Generalized chebyshev bandpass filters with frequency-dependent couplings based on stubs," *IEEE Trans. Microw. Theory Techn.*, vol. 61, no. 10, pp. 3601–3612, Oct. 2013.

[2] L. Szydlowski, A. Lamecki, and M. Mrozowski, "Coupled-resonator filters with frequency-dependent couplings: Coupling matrix synthesis," *IEEE Microw. Wireless Compon. Lett.*, vol. 22, no. 6, pp. 312–314, Jun. 2012.

[3] S. Tamiazzo and G. Macchiarella, "Synthesis of cross-coupled filters with frequency-dependent couplings," *IEEE Trans. Microw. Theory Techn.*, vol. 65, no. 3, pp. 775–782, Mar. 2017.

[4] Y. He, G. Macchiarella, G. Wang, W. Wu, L. Sun, L. Wang, and R. Zhang, "A direct matrix synthesis for in-line filters with transmission zeros generated by frequency-variant couplings," *IEEE Trans. Microw. Theory Techn.*, vol. 66, no. 4, pp. 1780–1789, Apr. 2018.

[5] S. Amari, M. Bekheit, and F. Seyfert, "Notes on bandpass filters whose inter-resonator coupling coefficients are linear functions of frequency," in *IEEE MTT-S Int. Microw. Symp. Dig.*, Jun. 2008, pp. 1207–1210.

[6] C.-L. Hsu and J.-T. Kuo, "Microstrip realization of trisection synthesis with frequency-dependent admittance inverter," *Prog. Electromagn. Res.*, vol. 113, pp. 195–210, Feb. 2011.

[7] J.-T. Kuo, Y.-C. Wang, and J.-W. Kuo, "Diplexer with trisections synthesized by frequency-dependent coupling," in *Proc. Asia–Pacific Microw. Conf. (APMC)*, vol. 3, Dec. 2015, pp. 1–3.

[8] X. Wu, X. Wei, and Y. Shi, "Design of a trisection wideband microstrip bandpass filter with frequency dependent coupling," in *Proc. 10th Int. Conf. Commun., Circuits Syst. (ICCCAS)*, Dec. 2018, pp. 136–139.

[9] A. Jedrzejewski, L. Szydlowski, and M. Mrozowski, "Accurate design of pseudoelliptic inline SIW filters with frequency-dependent couplings," in *Proc. 20th Int. Conf. Microw., Radar Wireless Commun. (MIKON)*, Jun. 2014, pp. 1–4.

[10] Q. Liu, D. Zhou, D. Zhang, and D. Lv, "A novel frequency-dependent coupling with flexibly controllable slope and its applications on substrate-integrated waveguide filters," *IEEE Microw. Wireless Compon. Lett.*, vol. 28, no. 11, pp. 993–995, Nov. 2018.

[11] W. Shen, L.-S. Wu, X.-W. Sun, W.-Y. Yin, and J.-F. Mao, "Novel substrate integrated waveguide filters with mixed cross coupling (MCC)," *IEEE Microw. Wireless Compon. Lett.*, vol. 19, no. 11, pp. 701–703, Nov. 2009.

[12] L. Szydlowski, N. Leszczynska, and M. Mrozowski, "Dimensional synthesis of coupled-resonator pseudoelliptic microwave bandpass filters with constant and dispersive couplings," *IEEE Trans. Microw. Theory Techn.*, vol. 62, no. 8, pp. 1634–1646, Aug. 2014.

[13] L. Szydlowski, N. Leszczynska, and M. Mrozowski, "A linear phase filter in quadruplet topology with frequency-dependent couplings," *IEEE Microw. Wireless Compon. Lett.*, vol. 24, no. 1, pp. 32–34, Nov. 2014.

[14] L. Szydlowski, A. Lamecki, and M. Mrozowski, "Coupled-resonator waveguide filter in quadruplet topology with frequency-dependent coupling—A design based on coupling matrix," *IEEE Microw. Wireless Compon. Lett.*, vol. 22, no. 11, pp. 553–555, Nov. 2012.

[15] L. Szydlowski and M. Mrozowski, "A self-equalized waveguide filter with frequency-dependent (Resonant) couplings," *IEEE Microw. Wireless Compon. Lett.*, vol. 24, no. 11, pp. 769–771, Nov. 2014.

[16] P. Zhao and K. Wu, "Cascading fundamental building blocks with frequency-dependent couplings in microwave filters," *IEEE Trans. Microw. Theory Techn.*, vol. 67, no. 4, pp. 1432–1440, Apr. 2019.

[17] Y. He, G. Macchiarella, Z. Ma, L. Sun, and N. Yoshikawa, "Advanced direct synthesis approach for high selectivity in-line topology filters comprising $N-1$ adjacent frequency-variant couplings," *IEEE Access*, vol. 7, pp. 41659–41668, 2019.

[18] S. Amari, "Synthesis of cross-coupled resonator filters using an analytical gradient-based optimization technique," *IEEE Trans. Microw. Theory Techn.*, vol. 48, no. 9, pp. 1559–1564, Sep. 2000.

[19] K. Lee, T.-H. Lee, Y.-S. Kim, and J. Lee, "New negative coupling structure for substrate-integrated cavity resonators and its application to design of an elliptic response filter," *Prog. Electromagn. Res.*, vol. 137, pp. 117–127, Feb. 2013.

[20] R. J. Cameron, "Advanced filter synthesis," *IEEE Microw. Mag.*, vol. 12, no. 6, pp. 42–61, Oct. 2011.

[21] C.-S. Ahn, J. Lee, and Y.-S. Kim, "Design flexibility of an open-loop resonator filter using similarity transformation of coupling matrix," *IEEE Microw. Wireless Compon. Lett.*, vol. 15, no. 4, pp. 262–264, Apr. 2005.

[22] J.-S. Hong and M. J. Lancaster, *Microstrip Filters for RF/Microwave Applications*, vol. 167. Hoboken, NJ, USA: Wiley, 2004.

[23] E. J. Naglich, J. Lee, D. Peroulis, and W. J. Chappell, "Bandpass-bandstop filter cascade performance over wide frequency tuning ranges," *IEEE Trans. Microw. Theory Techn.*, vol. 58, no. 12, pp. 3945–3953, Dec. 2010.

[24] S. Saeedi, J. Lee, and H. H. Sigmarsson, "Novel coupling matrix synthesis for single-layer substrate-integrated evanescent-mode cavity tunable bandstop filter design," *IEEE Trans. Microw. Theory Techn.*, vol. 63, no. 12, pp. 3929–3938, Dec. 2015.

[25] S. Nam, B. Lee, and J. Lee, "Theory for pseudo-butterworth filter response and its application to bandwidth tuning," *IEEE Trans. Microw. Theory Techn.*, vol. 65, no. 8, pp. 2847–2856, Aug. 2017.

[26] S. Nam, B. Lee, and J. Lee, "Reconfigurable bandpass filter topology using cul-de-sac resonators with adjustable notches," in *IEEE MTT-S Int. Microw. Symp. Dig.*, May 2016, pp. 1–4.

[27] T.-H. Lee, B. Lee, S. Nam, Y.-S. Kim, and J. Lee, "Frequency-tunable tri-function filter," *IEEE Trans. Microw. Theory Techn.*, vol. 65, no. 11, pp. 4584–4592, Nov. 2017.

[28] H. Joshi, H. H. Sigmarsson, S. Moon, D. Peroulis, and W. J. Chappell, "High-Q fully reconfigurable tunable bandpass filters," *IEEE Trans. Microw. Theory Techn.*, vol. 57, no. 12, pp. 3525–3533, Dec. 2009.

[29] B. Lee, B. Koh, S. Nam, T.-H. Lee, and J. Lee, "Band-switchable substrate-integrated waveguide resonator and filter," *IEEE Trans. Microw. Theory Techn.*, vol. 66, no. 1, pp. 147–156, Jan. 2018.
[30] B. Lee, S. Nam, T.-H. Lee, C.-S. Ahn, and J. Lee, "Single-filter structure with tunable operating frequency in noncontiguous bands," *IEEE Trans. Compon., Packag., Manuf. Technol.*, vol. 7, no. 1, pp. 98–105, Jan. 2017.
[31] G. Lee, B. Lee, J.-Y. Jeong, and J. Lee, "Ka-band surface-mount cross-coupled SIW filter with multi-layered Microstrip-to-GCPW transition," *IEEE Access*, vol. 7, pp. 66453–66462, 2019.
[32] S. Lee, S. Nam, B. Lee, and J. Lee, "Easy-to-fabricate embedded negative coupling structure for post-loaded dielectric resonator filter," in *Proc. 49th Eur. Microw. Conf. (EuMC)*, Oct. 2019, pp. 53–56.
[33] H. Wang and Q.-X. Chu, "An inline coaxial quasi-elliptic filter with controllable mixed electric and magnetic coupling," *IEEE Trans. Microw. Theory Techn.*, vol. 57, no. 3, pp. 667–673, Mar. 2009.

SANGGU LEE was born in Seoul, South Korea, in 1993. He received the B.E. degree in electronic engineering from Ajou University, Suwon, South Korea, in 2018. He is currently pursuing the Ph.D. degree in radio communications engineering from Korea University, Seoul, South Korea.

His current research interest includes post-loaded reflectionless filters.

SEUNGGOO NAM was born in Seoul, South Korea, in 1989. He received the B.E. degree in computer and communication engineering from Korea University, Seoul, in 2015, where he is currently pursuing the Ph.D. degree in radio communications engineering.

His current research interest includes K-band frequency tunable filters.

JUSEOP LEE (Senior Member, IEEE) received the B.E. and M.E. degrees in radio science and engineering from Korea University, Seoul, South Korea, in 1997 and 1999, respectively, and the Ph.D. degree in electrical engineering from the University of Michigan, Ann Arbor, MI, USA, in 2009.

In 2001, he joined the Electronics and Telecommunications Research Institute, Daejeon, South Korea, where he was involved in the design of passive microwave equipment for Ku- and Ka-band communication satellites. In 2005, he joined the University of Michigan, as a Research Assistant and a Graduate Student Instructor with the Radiation Laboratory, where he was involved in millimeter-wave radars and synthesis techniques for multiple-passband microwave filters. In 2009, he joined Purdue University, West Lafayette, IN, USA, as a Postdoctoral Research Associate, where he was involved in the design of adaptable RF systems. In 2012, he joined Korea University, where he is currently a Professor. Since August 2019, he has been a Visiting Professor with the University of Virginia, Charlottesville, VA, USA. His current research interests include RF and microwave components, satellite transponders, wireless power transfer, and electromagnetic theories.

Dr. Lee was a recipient of the Best Teaching Award presented by Korea University, in Spring 2018 and fall 2018. He was an Associate Editor of the IEEE TRANSACTIONS ON MICROWAVE THEORY AND TECHNIQUES, from 2017 to 2019.